ACADEMIC PRESS

Available online at www.sciencedirect.com

SCIENCE DIRECT®

Journal of Computational Physics 186 (2003) 481–502

JOURNAL OF COMPUTATIONAL PHYSICS

www.elsevier.com/locate/jcp

Electromigration of intergranular voids in metal films for microelectronic interconnects

Amir Averbuch [a,*], Moshe Israeli [b], Igor Ravve [c]

[a] *School of Computer Science, Tel Aviv University, Tel Aviv 69978, Israel*
[b] *Faculty of Computer Science, Technion, Haifa 32000, Israel*
[c] *Computing Science Department, Lawrence Berkeley Lab, University of California, CA, USA*

Received 19 March 2002; received in revised form 2 December 2002; accepted 19 January 2003

Abstract

Voids and cracks often occur in the interconnect lines of microelectronic devices. They increase the resistance of the circuits and may even lead to a fatal failure. Voids may occur inside a single grain, but often they appear on the boundary between two grains. In this work, we model and analyze numerically the migration and evolution of an intergranular void subjected to surface diffusion forces and external voltage applied to the interconnect. The grain–void interface is considered one-dimensional, and the physical formulation of the electromigration and diffusion model results in two coupled fourth-order one-dimensional time-dependent PDEs. The boundary conditions are specified at the triple points, which are common to both neighboring grains and the void. The solution of these equations uses a finite difference scheme in space and a Runge–Kutta integration scheme in time, and is also coupled to the solution of a static Laplace equation describing the voltage distribution throughout the grain. Since the voltage distribution is required only along the interface line, the two-dimensional discretization of the grain interior is not needed, and the static problem is solved by the boundary element method at each time step. The motion of the intergranular void was studied for different ratios between the diffusion and the electric field forces, and for different initial configurations of the void.

1. Introduction

Reliability of microelectronic circuits depends to a large extent on propagation of damages in the interconnect lines. Voids and cracks increase the resistance of the line and may even lead to open circuits, thus dramatically decreasing the lifetime of the device. Failures occur trough the void evolution, growth and motion, which are driven primarily by surface diffusion, electric field and mechanical stresses. Studies on grain–void interface dynamics and void morphology make it possible to predict the interconnect performance and eventually to improve the quality of a circuit design.

* Corresponding author. Tel.: +972-3-640-2020; fax: +972-3-640-9357.
E-mail address: amir@math.tau.ac.il (A. Averbuch).

0021-9991/03/$ - see front matter © 2003 Published by Elsevier Science B.V.
doi:10.1016/S0021-9991(03)00070-6

Voids often occur in grain boundaries, and thus, studying and modeling their surface diffusion and electromigration phenomena requires some intergranular analysis [1]. In this paper, we develop a numerical approach to track the dynamics of the void motion under the action of diffusion forces and an external voltage. Mechanical stresses are not treated in this paper. Consider a curved line, which separates the grain from the void. The basic assumption is that the interface moves in its normal direction with a known velocity function F. The tangential motion is usually neglected when a void inside a single grain is considered. For an intergranular void, the tangential motion is allowed along with the normal motion in the proximity of triple points, which belong to each of the two grains and to the void. Otherwise, the boundary conditions cannot be satisfied. The front velocity is caused by the surface diffusion and the electromigration components, depending on the second derivatives of the interface curvature K and of the voltage U [2,3], respectively. The derivatives are taken with respect to the interface arclength s:

$$F = BK_{ss} + \alpha U_{ss}. \tag{1}$$

The positive coefficients B and α express the contributions of the diffusion forces and the field forces, respectively. They depend on the properties of the material, temperature, etc. and are considered here to be material constants. We assume further that the time is normalized so that $B = 1$.

The structure of the paper is as follows. In Section 2 we review some of the central works on electromigration in thin metallic films. In Section 3 we derive the physical formulation of the two grain metallic film problem. We consider the motion of triple points and the continuity conditions at the triple joints. We distinguish between a general case and a symmetric void where the axis of symmetry coincides with the grain boundary line and with the direction of the external electric field. In Section 4 we give a finite difference formulation for the diffusion component of the normal velocity of the interface. We consider first a general internal point of the interface and then specifically a triple point, referring both to the normal and the tangential motion at the proximity of the triple point. In Section 5 we consider the elliptic equation for distribution of the electric potential and formulate its boundary conditions. The numerical results are presented in Section 6.

2. Electromigration in thin films: review

Predictions for dynamics and evolution of voids and cracks in thin metallic films of interconnect lines have a practical importance for microelectronics technology, and many researchers have contributed to this study. In this section we review what we consider as the most essential. Xia et al. [8] introduced a two-dimensional finite element method to compute the motion and evolution of a void in a single grain by surface diffusion in an elastic, electrically conductive solid. They accounted for the influence of deformation, electric current flow and effects of mass flow. The methodology has been used to predict the conditions of failure of the interconnect. A three-dimensional finite element model for studying the motion and evolution of voids in an idealized interconnect line due to electromigration- and strain-induced surface diffusion have been developed by Zhang et al. [9] to predict more accurately the behavior of the void. The spatial finite element formulation has been further exploited by Zhang and Bower [10] to study the conditions for formation of islands in a thin film of semiconductor material. Kraft et al. [11] presented the results of experimental studies of the mechanical behavior of thin films. Films on the silicon and polymer substrates were strained, and the film stress was determined by X-ray measurements.

Kraft and Arzt [20] examined electromigration mechanisms in conductor lines, applying finite difference and finite element formulations and compared the results of numerical simulations with experimental studies. They analyzed an electromigration damage in unpassivated aluminum-based interconnect lines and discovered that slit-like voids in bamboo lines develop from equi-axed voids through a shape change driven

by the "electron wind", taking into account the finite width of the line, surface tension effects and anisotropic diffusivity. Further, Kraft and Arzt [22] developed a model to predict lifetimes of conductor lines and to describe the microscopic damage behavior, considering nucleation and growth of electromigration voids. The reliability of a bamboo line is governed by the critical current density.

Experimental and theoretical studies of aluminum interconnects that include copper as an alloying element were carried out by Spolenak et al. [21]. A mechanistic model was developed to account for an increase in activation energies for aluminum drift in alloys in comparison to the pure metal, and this approach was in good agreement with the experiments. Copper as an alloying element improves strongly the electromigration resistance of the interconnects and thus reduces the damage caused by evolution and growth of voids.

Gungor and Maroudas in a series of papers [12,13,23,26,31–33] and with collaborators [25] studied the complex of linear and non-linear dynamics and stability of transgranular voids in thin films with bamboo grain structure. They simulated [12] the formation of various morphological features: void faceting, formation of wedge-shaped void, propagation of slit-like and soliton-like features and open-circuit failures. In [13] they performed a theoretical analysis for conditions of failure of metallic films. The dynamics of void is governed by a surface mass transport, electric field, elastic and plastic deformations. Anisotropic properties are taken into account in surface diffusivity and stresses. In [33] they applied a linear stability theory to examine the effects of anisotropy in surface diffusion. In [32] they performed a theoretical analysis and numerical simulations of the effects of residual stress on the failure mechanisms of passivated metallic thin films and observed two modes of failure to occur concurrently during void morphological evolution: electromigration-induced formation of faceted slits and stress-induced formation of fine-scale crack-like features on the void surface. In [31] current-induced morphological evolutions of void surfaces were studied theoretically and numerically, accounting for surface diffusional anisotropy. The non-linear analysis predicted a surface morphological transition and the onset of oscillatory dynamics at a critical strength of the applied electric field. Migration of voids along the film at constant speed with steady and time-periodic surface morphologies was studied, for electric fields weaker and stronger than critical. In a recent study [23] a multiscale modeling approach for the analysis of morphological evolution and electromigration failure in ductile metallic thin films of integrated circuits was presented. The effect of anisotropy of void surface diffusivity on the stability of the interconnects was presented in [26]. They predicted formation of stable faceted voids and wedge-shaped voids and studied failure due to propagation of slit-like features from void surfaces. In [25] they considered morphological instabilities caused by simultaneous action of applied mechanical stress and electric field on transgranular dynamics of voids, and studied propagation of slits. They predicted by numerical simulations that a failure might occur by the coupling of two modes of surface morphological instability. The above serious, extensive broad analysis was very instrumental for the design of integrated circuits by allowing to predict the reliability and the lifetime of the interconnect.

Schimschak and Krug [28] proposed a continuum description of the surface evolution that takes into account electromigration and capillarity-driven surface diffusion. They applied for numerical simulations a one-dimensional model of interface dynamics, which can be parameterized by a height function. The one-dimensional geometry is convenient and relevant to the modeling of shape changes at the edge of an effectively two-dimensional conductor line, but becomes inappropriate if the dynamics creates overhangs. In [27] they studied numerically the motion and shape evolution of an infinitely extended, isotropic and homogeneous two-dimensional current carrying conductor, considering a series of morphological transitions and conditions of instability for initially circular voids. The electromigration-induced shape evolution of cylindrical voids was numerically examined in [14], accounting for mass transport, current crowding and crystal anisotropy in the surface mobility. The authors considered finite strips with periodic boundary conditions in the current direction and voids in infinite or semi-infinite strips.

Mahadevan et al. [15] studied an edge instability in single-crystal metal lines, applying a numerical phase field technique. The authors defined the critical value of the applied current when the edge perturbation grows to become a slit-shaped void that spans the wire and leads to electrical failure, reducing the circuit lifetime to an unacceptable level. The phase field model [16] provides an attractive alternative to these techniques in which the interface is not explicitly tracked. In the phase field approach, the idea of a sharp interface between metal and void is abandoned. Instead, the thin film and the space around it are described by a continuous and but rapidly varying scalar function, called an order parameter. It accepts specific distinct uniform values well within the metal and well inside the void.

There is an apparent analogy between the level set method [4,5,7,41–44] and phase field method. In the level set, the level function is usually a signed distance from the given point to the interface line. The distance is considered negative in the void and positive in the conducting medium. Applying the hyperbolic tangent to the scaled distance function, one gets a parameter of phase field. Indeed, this leads to unity well inside a metal and minus unity well in a void. The scaling parameter adjusts the rapidly or slowly varying function.

Mahadevan and Bradley [29] used a phase field method to simulate the time evolution of a perturbation to the edge of current-carrying, single-crystal metal line, accounting for electromigration, surface diffusion and current crowding. The authors provided a fabrication criterion which ensured that the wire will not fail through formation of voids. In this case the edge perturbations are small enough so that the operating current does not exceed the threshold, and the instability through the formation slit-shaped voids does not occur. An alternative approach to increase the lifetime of the interconnect is to orient appropriately the crystal with respect to the applied field.

The phase field principle with an order parameter characterizing the damaged state of the interconnect was further used by Bhate et al. [17,30] for simulating electromigration- and stress-induced void evolutions. The evolution of the order parameter was governed by a fourth-order parabolic PDE, related to the Cahn–Hilliard equation [18]. Bhate et al. solved the PDE by an implicit finite element scheme together with the accompanying mechanical (elastic) and electrical problems.

Fridline and Bower [19] studied the effect of the anisotropy of the surface diffusivity on the formation and growth of slit-like voids, considering an interconnect as a two-dimensional electrically conducting strip that contains an initial semi-circular void. They applied a finite element model to predict the evolution of the void after an electric field was applied to the strip. Their later work [24] accounts for several kinetic processes involved in interconnect failures, including surface diffusion, interface and grain boundary diffusion, sliding on grain boundaries and at the interface between line and elastic passivation.

Gray et al. [34] applied an approximate Green's function to solve the Laplace equation for the electric potential by boundary element method in order to model the void dynamics under electromigration conditions in metallic thin-film interconnects used in integrated circuits. The approximate Green's function was constructed by reflecting the source point through a plane. The method retains the primary attribute of an exact Green's function: elimination of surfaces from the calculation. Another application of the method is the simulation of the industrial electroforming process.

Suo [36] considered aluminum interconnects in the presence of insulators and shunts, subjected to temperature change and a direct electric current. He studied the evolution of interconnects, into a stable state with a segment of aluminum depleted near the cathode, a linear distribution of pressure in the rest of the line, and no further mass diffusion, and estimated the time scale for the interconnect to evolve to the stable state. In [35] the mechanisms for diffusive processes in solid structures of small feature sizes, between a few to hundreds of nanometers, were described. Considering microelectronic and fotonic devices, he applied the concept of free energy. The change of free energy defines a thermodynamic force, which in its turn drives the configurational change of the structure. The author gives a physical description of forces of diverse origins, that occur in thin films of interconnect lines, including elasticity, electrostatics, capillarity, electric current and others. Yu and Suo [37] derived a finite element formulation to model the dynamics of a

single pore on a moving grain boundary, assuming that surface diffusion is the dominant process for a small pore to adjust its shape and position.

Sun et al. [38] considered the evolution of grains in a polycrystalline fiber and applied a variational approach to microstructure development, which incorporates thermodynamic forces and mass transport mechanisms. The free energy includes interfacial, elastic, electrostatic and chemical components. The rate process includes diffusion, creep, grain-boundary motion and surface or interface reactions. In a later work, Sun et al. [39] modeled the dynamics of a two-grain thin film on a substrate. They developed a finite element formulation that accounted for surface tension anisotropy, bulk phase free energy density and finite junction mobility. The authors formulated the laws for the motion and equilibrium of triple junctions and considered the motion of grain–void interfaces and grain boundary. The large shape changes of a solid due to matter diffusion on its surface were studied by Sun and Suo [40]. In addition to surface diffusion, evaporation and condensation were accounted for, and the finite element approach was applied to analyze the thermal grooving on a polycrystalline surface.

An electromigration problem with a specific geometry is solved in our study by a different numerical approach. We applied a parametric presentation of the curved interface between external void and the bulk material in the Cartesian space. In addition, the application of the cubic spline technique to rearrange the generating points of the interface line in a uniform manner allows to apply the standard methods of finite difference of any order. We assume that the boundary between the two grains was parallel to the direction of the external electric field and that the void was symmetric relative to this boundary. With this approach one may omit continuous or systematic application of the remeshing and elimination procedure on the irregularly disposed nodes.

3. Physical formulation

3.1. Angles at triple points

Consider a grain boundary that is split by the void into two sections as shown in Fig. 1(a). The vector $\boldsymbol{E}$ denotes the direction of the electric field. The void migrates and evolves under surface diffusion and electric field forces. We assume for simplicity that the grain boundaries A_0A_1A and B_0B_1B contribute no additional electric resistance, and suppose that the specific resistance of both grains is the same.

We assume that mechanical equilibrium holds at the triple points A and B. The specific surface energy (per unit length of of the grain–void boundary) is the same for grains 1 and 2. Therefore, at the triple

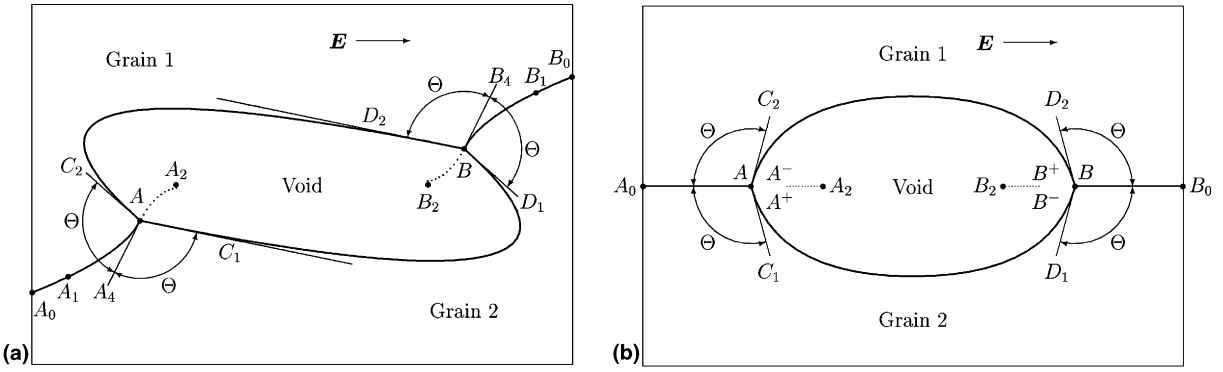

Fig. 1. Two grain scheme: (a) general; (b) symmetric.

points, the angles Θ between the tangent line to the intergranular boundary and the tangent lines to the void interface contour are the same

$$\angle C_1AA_1 = \angle C_2AA_1 = \Theta, \quad \angle D_1AA_1 = \angle D_2AA_1 = \Theta. \tag{2}$$

The value of these angles is defined by

$$\Theta = \frac{\pi}{2} + \arcsin\frac{\gamma_{GB}}{\gamma_S} \approx \frac{\pi}{2} + \frac{\pi}{12} = \frac{7\pi}{12}, \tag{3}$$

where γ_{GB} is the specific grain boundary energy and γ_S is the specific surface energy. We assume here that Eq. (2) holds at start time (for the initial configuration) and during the void motion as well. We do not account for dynamical changes of the triple angles.

3.2. Migration of triple points

The triple points A and B can move either along the "old" grain boundaries AA_1 and BB_1, which exist already in the initial configuration, or along the "new" grain boundaries AA_2 and BB_2, which did not exist before. The configuration of the boundary between the grains varies with time. The motion of the triple points in the outward direction is permitted along the existing boundary paths only. The motion of the triple points inward of the void is accompanied by creating the new paths. One may suppose that when the void migrates often one of the triple points moves in the inward direction, and another one moves in the outward direction.

3.3. Continuity of the flux

The main physical condition, which holds at the triple points, is the continuity of the flux

$$I_o = I_s^+ - I_s^-, \tag{4}$$

where I_o is the flux along the grain boundary, and I_s are the fluxes along the grain–void interface. The superscript '−' denotes the location on this interface immediately before the triple point, and '+' immediately behind, passing the void contour in the counterclockwise direction. In other words, the diffusion flux along the grain boundary equals to the change of the diffusion flux when we pass from the interface of the void in the first grain to that in the other grain. The diffusion flux for any point in the surface is

$$I_s = K_s + \alpha U_s, \tag{5}$$

where subscript s means the derivative with respect to the arclength on the grain–void interface. By substituting Eq. (5) into (4) we have

$$I_o = K_s^+ - K_s^- + \alpha(U_s^+ - U_s^-), \tag{6}$$

where U_s^- and U_s^+ are considered as known values, established by the electrostatic problem.

Assume conductivity of the void is zero. In this case, the derivative of voltage vanishes in two different directions: normal to grain 1 and normal to grain 2 (see Fig. 1). This means that the voltage gradient vector at the triple points vanishes, so that the derivative of the voltage is zero in any direction, in particular, in the direction tangent to the grain–void interface. Thus, Eq. (5) reduces to

$$I_s = K_s, \tag{7}$$

i.e., for the zero conductivity of the void, the diffusion flux at the triple point is equal to the derivative of the curvature with respect to arclength. Now Eq. (4) leads to

$$I_o = K_s^+ - K_s^-. \tag{8}$$

The diffusion flux along the grain boundary is constant since we assume that there is no accumulation or depletion of material along this boundary

$$I_o = \frac{\beta}{\alpha} U_{\mathrm{g}} - \gamma S_{\mathrm{g}}, \tag{9}$$

where U_{g} is the derivative of the voltage along the grain boundary, S_{g} is the derivative of the stress, β and γ are constant coefficients depending on the elastic and the electro-chemical properties of the material.

Continuity means that the flux I_o at infinity is equal to the flux at the triple point. Since there are no stresses at infinity, the flux there is proportional to the external electric field

$$I_o^{\infty} = \frac{\beta}{\alpha} \frac{\Delta U}{L}, \tag{10}$$

where ΔU is the applied external voltage, and L is the total length of the metallic line. Finally, we get a boundary condition at the triple point

$$K_s^+ - K_s^- = \frac{\beta}{\alpha} \frac{\Delta U}{L}. \tag{11}$$

3.4. Symmetric void

In the present work we consider a simple particular two-grain symmetric problem. The interganular boundary is assumed to be a straight horizontal line, and the void is symmetric with respect to this line. In this case, only the upper half of the void interface has to be considered. The symmetric scheme is presented in Fig. 1(b). For a symmetric void, the curvature K is an even function of the arclength with respect to the triple point, and its derivative is an odd function

$$K_s^- = -K_s^+. \tag{12}$$

The continuity equation (11) becomes

$$K_s(A^-) = K_s(B^+) = \frac{\beta}{\alpha} \frac{\Delta U}{2L}. \tag{13}$$

Eq. (13) refers to the triple points of the upper half of the symmetric grain boundary.

3.5. Non-symmetric void

Eq. (12) does not hold for a non-symmetric void. We need an additional condition to establish K_s^+ and K_s^-. This condition is the identity of the interface velocities in the triple point at '+' and '−'. Projections of these velocities on the direction of the grain boundary should be the same, otherwise the triple point does not exist. Since the triple angles are the same for both branches of the interface, then there is a continuity of the front velocity

$$F^+ = F^- \quad \text{or} \quad K_{ss}^+ - K_{ss}^- = -\alpha(U_{ss}^+ - U_{ss}^-), \tag{14}$$

where the right-hand side of the last equation is assumed to be a known value and can be established from the electrostatic problem.

4. Finite difference formulation of diffusion component

4.1. Internal points

Assume that the void boundary is set parametrically in the Cartesian space

$$x = x(r), \quad y = y(r), \tag{15}$$

where r is a parameter which is independent of time. The evolution equations [5] are

$$\dot{x} = F\frac{y'}{g}, \quad \dot{y} = -F\frac{x'}{g}, \tag{16}$$

where the dot denotes time derivative and the prime denotes the spatial derivative (with respect to the parameter r). The current arclength cannot be used as a parameter since it is time-dependent, but the arclength of the initial configuration or other reference configuration can be used. g is the metric and is defined by

$$g = \frac{\mathrm{d}s}{\mathrm{d}r} = \sqrt{x'^2 + y'^2}. \tag{17}$$

F is the normal velocity of the front defined by Eq. (1). It depends on the second derivative of the curvature and that of the voltage with respect to the current arclength. The voltage distribution will be discussed in Section 5. The second derivative of the curvature with respect to the arclength is

$$K_{ss} = \frac{\mathrm{d}K_s}{\mathrm{d}s} = \frac{\mathrm{d}r}{\mathrm{d}s}\frac{\mathrm{d}K_s}{\mathrm{d}r} = \frac{1}{g}\frac{\mathrm{d}}{\mathrm{d}r}\frac{K'}{g} = \frac{K'' - K'g'}{g^3}. \tag{18}$$

From Eq. (17) it follows that

$$g' = \frac{x'x'' + y'y''}{g}, \tag{19}$$

g and g' are not new functions but new notation. The curvature K is defined as

$$K = \frac{y''x' - x''y'}{g^3}. \tag{20}$$

Thus, the governing set (Eq. (16)) contains two coupled PDEs of fourth- order in space and first-order in time.

Assume that the interface line is set initially by a sequence of generating points $(x_0, y_0), (x_1, y_1), \ldots, (x_N, y_N)$, not necessarily equally spaced. We would like to create a parametric presentation of the interface line, and at first, we use as a parameter the normalized number of the current point i/N. At this point we introduce the cubic spline interpolation by considering the generating points as the nodes of the cubic spline. Thus, we are able to compute the arclength along the interface line and to redistribute the generating points in a uniform equidistant manner. Now we use the arclength of the initial configuration as a parameter

$$x_i = x(s_i), \quad y_i = y(s_i), \quad s_i - s_{i-1} = \Delta s = \text{const}. \tag{21}$$

At the ends of the spline, the derivative boundary conditions are applied because the slopes of the interface are known at the triple points. Note that the arclength of the current configuration depends on time while that of the initial configuration obviously does not. Since the arclength is used as a parameter, then at $t = 0$, the metric is identically unity, and its spatial (arclength) derivative vanishes everywhere

$$g(s) \equiv 1, \quad g'(s) = 0. \tag{22}$$

Relation (22) is used when we start the first step in time.

The governing equations are of fourth-order in space. For the arclength used as a parameter, the second derivative of the curvature becomes

$$K_{ss} = (y''x' - x''y')'' = y^{\mathrm{IV}}x' - x^{\mathrm{IV}}y' + y'''x'' - x'''y''. \tag{23}$$

However, instead of direct calculation of the third and fourth derivatives, it is suitable to establish the first and second derivatives of the Cartesian components in order to approximate the curvature, and then to calculate the second derivative of the curvature. For all grid points, except the triple points ($s = 0$ and $s = S_{\max}$) and the nodes immediately adjacent to the triple points ($s = \Delta s$ and $s = S_{\max} - \Delta s$), the central differences can be applied:

$$\begin{aligned}
x'(s) &= \frac{x(s+\Delta s) - x(s-\Delta s)}{2\Delta s},\\
y'(s) &= \frac{y(s+\Delta s) - y(s-\Delta s)}{2\Delta s},\\
x''(s) &= \frac{x(s+\Delta s) - 2x(s) + x(s-\Delta s)}{\Delta s^2},\\
y''(s) &= \frac{y(s+\Delta s) - 2y(s) + y(s-\Delta s)}{\Delta s^2},\\
K(s) &= y''(s)x'(s) - x''(s)y'(s),\\
K''(s) &= \frac{K(s+\Delta s) - 2K(s) + K(s-\Delta s)}{\Delta s^2}.
\end{aligned} \tag{24}$$

The scheme is of second-order accuracy, and the local truncation error for the second derivative of the curvature proves to be

$$E = \left(y'''x^{\mathrm{IV}} - x'''y^{\mathrm{IV}} + 3y''x^{\mathrm{V}} - 3x''y^{\mathrm{V}} + 2y'x^{\mathrm{VI}} - 2x'y^{\mathrm{VI}}\right)\frac{\Delta s^2}{12}. \tag{25}$$

4.2. Triple points and neighboring nodes

Boundary condition should be used for triple points and adjacent nodes. To find the second derivative of the curvature, we apply the one-sided (forward or backward) difference, using the values of the curvature and the given value of its derivative at the triple point. Assume that a second-order accuracy is required for the second derivative of the curvature at the end points too. Nodes 0 and N are triple points, nodes 1 and $N-1$ are adjacent nodes.

For a uniform symmetric grid, the finite difference approximation of the second derivative with the second-order accuracy contains three node values. However, we cannot apply the symmetric formula for node 0, and since the grid ceases to be symmetric, additional node value is required. This will be the node value of the first derivative of the curvature at the triple point. We introduce the following notation: A and B are the triple points, a and b are the corresponding adjacent nodes. Let us seek the difference scheme in the following form:

$$K_{ss}^{A} = \frac{C\Delta s K_s^A + C_0K_0 + C_1K_1 + C_2K_2}{\Delta s^2}, \tag{26}$$

where C, C_0, C_1 and C_2 are the coefficients to be established. The error should be of order Δs^2. We expand K_1 and K_2 into Taylor series in the proximity of the triple point A till $O(\Delta s^4)$ neglecting the high order terms:

$$\begin{aligned} K_1 &= K(s+\Delta s) = K_0 + K_0'\Delta s + \frac{K_0''\Delta s^2}{2} + \frac{K_0'''\Delta s^3}{6} + \frac{K_0^{(4)}\Delta s^4}{24}, \\ K_2 &= K(s+2\Delta s) = K_0 + 2K_0'\Delta s + 2K_0''\Delta s^2 + \frac{4K_0'''\Delta s^3}{3} + \frac{2K_0^{(4)}\Delta s^4}{3}. \end{aligned} \tag{27}$$

Substituting Eq. (27) into (26) and balancing the terms, we get the following solution:

$$\begin{cases} C_0 + C_1 + C_2 = 0, \\ C + C_1 + 2C_2 = 0, \\ C_1 + 4C_2 = 2, \\ C_1 + 8C_2 = 0, \end{cases} \quad \begin{cases} C = -3, \\ C_0 = -7/2, \\ C_1 = 4, \\ C_2 = -1/2. \end{cases} \tag{28}$$

Thus, the difference approximation and the leading error term become

$$K_{ss}^A = \frac{-6\Delta s K_s^A - 7K_0 + 8K_1 - K_2}{2\Delta s^2} - \frac{K_0^{(4)}\Delta s^2}{6}. \tag{29}$$

The higher order terms are neglected. Of course, the error is not a total truncation error, as the values of the curvature in Eq. (29) are not exact. Additional error terms will be computed later. The central difference for K_{ss}^a can be used

$$K_{ss}^a = \frac{K_0 - 2K_1 + K_2}{\Delta s^2} - \frac{K_1^{(4)}\Delta s^2}{12}. \tag{30}$$

If we desire to get a truncation error $O(\Delta s^2)$, then the values of K_0, K_1 and K_2 should be estimated with the accuracy $O(\Delta s^4)$. This means that the first and the second derivatives of x and y at these points should be of the fourth-order accuracy.

The first derivatives x' and y' at the triple point are set exactly. Similar technique of undetermined coefficients that was used for the second derivative of the curvature yields the first derivatives at two other points:

$$\begin{aligned} x_1' &= \frac{-6\Delta s x_A' - 17x_0 + 9x_1 + 9x_2 - x_3}{18\Delta s} - \frac{x_1^{(5)}\Delta s^4}{60}, \\ x_2' &= \frac{3\Delta s x_A' + 7x_0 - 18x_1 + 9x_2 + 2x_3}{9\Delta s} + \frac{x_2^{(5)}\Delta s^4}{30}. \end{aligned} \tag{31}$$

The second derivatives are:

$$\begin{aligned} x_0'' &= \frac{-300\Delta s\, x_A' - 415x_0 + 576x_1 - 216x_2 + 64x_3 - 9x_4}{72\Delta s^2} - \frac{x_0^{(6)}\Delta s^4}{15}, \\ x_1'' &= \frac{60\Delta s\, x_A' + 257x_0 - 480x_1 + 252x_2 - 32x_3 + 3x_4}{144\Delta s^2} + \frac{x_1^{(6)}\Delta s^4}{360}, \\ x_2'' &= \frac{-x_0 + 16x_1 - 30x_2 + 16x_3 - x_4}{12\Delta s^2} - \frac{x_2^{(6)}\Delta s^4}{90}. \end{aligned} \tag{32}$$

Similar equations are used for derivatives of y. We calculate the curvature using the first and the second derivatives of x and y and get the following truncation errors:

$$
\begin{aligned}
E(K_0) &= \frac{y_0' x_0^{(6)} - x_0' y_0^{(6)}}{15}\,\Delta s^4,\\
E(K_1) &= \frac{-y_1' x_1^{(6)} + x_1' y_1^{(6)} - 6y_0'' x_1^{(5)} + 6x_0'' y_1^{(5)}}{360}\,\Delta s^4,\\
E(K_2) &= \frac{y_2' x_2^{(6)} - x_2' y_2^{(6)} + 3y_2'' x_2^{(5)} - 3x_2'' y_2^{(5)}}{90}\,\Delta s^4.
\end{aligned}
\tag{33}
$$

The additional error terms that estimate the second derivative of the curvature are

$$
\begin{aligned}
E(K_{ss}^A) &= \frac{-3y_0' x_0^{(6)} + 3x_0' y_0^{(6)} - y_0'' x_0^{(5)} + x_0'' y_0^{(5)}}{12}\,\Delta s^2,\\
E(K_{ss}^a) &= \frac{5y_1' x_1^{(6)} - 5x_1' y_1^{(6)} + 4y_1'' x_1^{(5)} - 4x_0'' y_1^{(5)}}{60}\,\Delta s^2.
\end{aligned}
\tag{34}
$$

These values are added to the principal error terms in Eqs. (29) and (30), respectively. For the other end with triple point B and neighbor point b, the difference approximations are derived in a similar manner.

4.3. Tangential motion at the proximity of triple points

The illustrative scheme for tangential motion is presented in Fig. 2. A and B are the positions of the triple points before marching in time. Marching in time takes into consideration the normal motion of the curve only. Therefore, after the completion of one-step march, the new locations A' and B' of the old triple points may prove to be either above or below the horizontal grain boundary, depending on the sign of the front velocity. These are not true triple points as they do not belong to the interface between two grains. Assume, for example, that $F^A > 0$ and $F^B < 0$, i.e., the front velocity is positive at A and negative at B. In Fig. 2 the solid line is the grain–void boundary before marching, the dot line is the grain–void boundary after marching. The vectors AA' and BB' are normal shifts of the triple points, and they are fairly small with respect to the arclength grid since $\Delta t \sim \Delta s^4$, due to stability requirements of the explicit difference scheme. For the new grain–void interface line, we apply the spline interpolation technique with the derivative boundary conditions at the end of the spline. We use extrapolation when the new end point A' is above the grain boundary, and interpolation when the end point B' is below that boundary. Since the normal shifts are fairly small with respect to the spline grid, the interpolation or extrapolation points are very close to the end nodes of the spline, and the accuracy of the extrapolation is good. We solve the spline equations $y(s) = 0$ at the proximity of the triple points, using the initial guess $s = 0$ and $s = S_{\max}$ for points A'' and B'', respectively. Thus, we find the corresponding values of s and $x(s)$. Now the ends of a new grain–void interface are located at the grain boundary, and we rearrange the spline for these new ends.

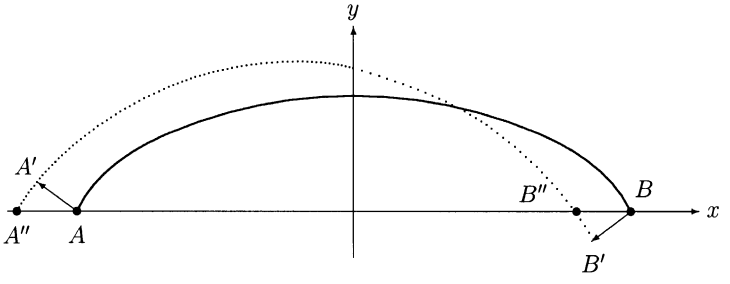

Fig. 2. Tangential motion of interface line.

4.4. Runge–Kutta integration scheme

The explicit Runge–Kutta scheme is applied on marching in time. Since the governing PDEs are of the fourth-order in space, the time step should be limited to provide a stable integration

$$\Delta t = k_z \frac{\Delta s^4}{B}, \tag{35}$$

where k_z is a dimensionless coefficient. Numerical simulations show that for the governing PDEs (1) it should not exceed 1/35, assuming $B = 1$. Since the time step, which is defined by stability requirements is very small, there is no need to apply Runge–Kutta schemes of high orders. Therefore, we use order 2. After discretization in space, the two PDEs become a set of ODEs

$$\begin{cases} \dot{x}_i = \left[K_i''(\boldsymbol{x},\boldsymbol{y}) + \alpha U_i''(\boldsymbol{x},\boldsymbol{y})\right] y_i' \stackrel{\text{def}}{=} f_i(\boldsymbol{x},\boldsymbol{y}), \\ \dot{y}_i = -\left[K_i''(\boldsymbol{x},\boldsymbol{y}) + \alpha U_i''(\boldsymbol{x},\boldsymbol{y})\right] x_i' \stackrel{\text{def}}{=} \mathrm{h_i}(\boldsymbol{x},\boldsymbol{y}). \end{cases} \tag{36}$$

Runge–Kutta of the second order yields the following scheme:

$$\begin{cases} \tilde{x}_i(t+\Delta t) = x_i + f_i(\boldsymbol{x},\boldsymbol{y})\Delta t, \\ \tilde{y}_i(t+\Delta t) = y_i + h_i(\boldsymbol{x},\boldsymbol{y})\Delta t, \\ \begin{cases} x_i(t+\Delta t) = x_i + \frac{f_i(\boldsymbol{x},\boldsymbol{y}) + f_i(\tilde{\boldsymbol{x}},\tilde{\boldsymbol{y}})}{2}\Delta t, \\ y_i(t+\Delta t) = y_i + \frac{h_i(\boldsymbol{x},\boldsymbol{y}) + h_i(\tilde{\boldsymbol{x}},\tilde{\boldsymbol{y}})}{2}\Delta t. \end{cases} \end{cases} \tag{37}$$

After each step we rearrange the spline so that the generating points of the new interface are equally spaced discretization of the new arclength. Therefore, at the beginning of each step, the arclength may be considered as the arclength of the initial configuration, and can be treated as time-independent parameter. The ambiguity with variable arclength arises at the second sweep of the Runge–Kutta scheme. Indeed, the functions $f_i(\tilde{\boldsymbol{x}},\tilde{\boldsymbol{y}})$ and $g_i(\tilde{\boldsymbol{x}},\tilde{\boldsymbol{y}})$ are based on the derivatives of the parameter which is not an arclength any more. Thus, the new metric $g = \sqrt{x'^2 + y'^2}$ should be introduced, and a formulae for an arbitrary parameter that includes this metric should be used. We neglect this fact and assume that the parameter is still an arclength on the second sweep of the Runge–Kutta scheme. Strictly speaking, this means that the integration scheme that we use is not exactly Runge–Kutta of the second order. It is more accurate than the Euler scheme, but less accurate than the perfect Runge–Kutta of the second order.

5. Distribution of voltage

The voltage distribution is required only along the interface line. Therefore, we use the boundary element approach to avoid discretization of the interior domain. We deal with a static problem, and the boundary integral reduces the two-dimensional problem to one-dimensional problem. The conductivities of the two grains are assumed equal and constant throughout the grain domains. Conductivity of the void is different and also constant within the void. We consider here two different formulations for the problem: (1) A simplified case with infinite resistance of the void. (2) A general case with a finite resistance of the void (defined by properties of the underlayer).

For a medium with a varying conductivity $k(x,y)$, the voltage distribution $U(x,y)$ is governed by an elliptic PDE [7]

$$\frac{\partial}{\partial x}\left[k(x,y)\frac{\partial U}{\partial x}\right]+\frac{\partial}{\partial y}\left[k(x,y)\frac{\partial U}{\partial y}\right]=0. \tag{38}$$

The distribution of the voltage inside a homogeneous medium of constant resistance is described by the Lapalce equation with the Dirichlet and Neumann boundary conditions. For a multi-phase medium of a piecewise-homogeneous resistance, the voltage distribution is governed by the Laplace equation inside each phase, with the Dirichlet and Neumann boundary conditions at the external boundaries and equations of compatibility along the interface lines between the phases of different conductivity. The boundary conditions are shown in Fig. 3(a) for a non-conducting void. The scheme for a 'void' with finite conductivity (which is due to the substrate) is presented in Fig. 3(b).

Consider the case where the void has infinite resistance. The value of the potential is set at the vertical boundaries of the interconnect: $U = U^+$ at the left side A_0F and $U = U^-$ at the right side B_0G. Along the upper side FG the normal derivative of voltage vanishes as this is the external boundary of the interconnect line. Along the lower sides A_0A and BB_0 the derivative U_n vanishes due to the symmetry of the problem. Along the arc AEB it vanishes due to the infinite resistance of the void.

Now we consider a void of finite resistance. Let k_g and k_v be the conductivities of the grain material and the void, respectively. When the conductivity of the medium varies in a discontinuous manner, the voltage is still a continuous function (a finite single-valued potential exists at any point), but there is a jump in the voltage derivative normal to the interface line between the two media. Thus, there are two conditions for the compatibility

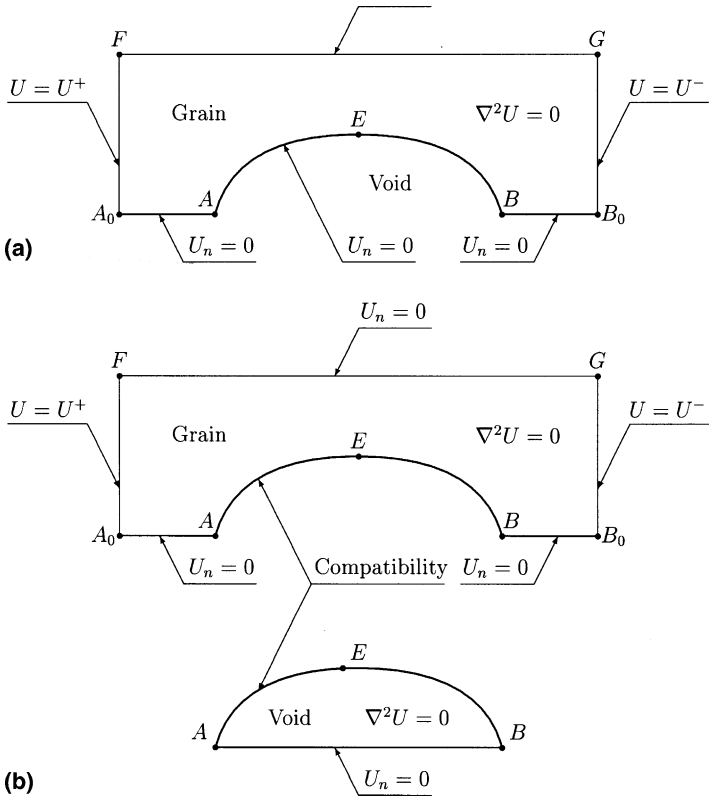

Fig. 3. Boundary conditions for the voltage distribution problem: (a) infinite resistance of the void; (b) finite resistance of the void.

$$U^{g} = U^{v}, \quad k_{g}U_{n}^{g} + k_{v}U_{n}^{v} = 0, \tag{39}$$

where U^{g} is the voltage at the grain–void interface for the points that belong to the grain; U^{v} is that for the interface points that belong to the void. These are the same points, and the same voltage. U_{n}^{g} is the voltage derivative in the direction of the outward normal to the grain; U^{v} is that in the direction of the outward normal to the void.

Application of the boundary integral method reduces the Laplace equation to the integral equation

$$U(\xi) = \frac{1}{\pi - \alpha_{\xi}} \oint \left[\frac{\partial \ln R(\xi, \Gamma)}{\partial n} U(\Gamma) - U_{n}(\Gamma) \ln R(\xi, \Gamma) \right] d\Gamma, \tag{40}$$

where ξ is the given point of the boundary; $\alpha_{\xi} = 0$ if the boundary is smooth at that point, and $\alpha_{\xi} = \alpha^{+} - \alpha^{-}$ is the change in the direction of the tangent line if there is a sharp angle; $R(\Gamma, \xi)$ is the radius vector from the given fixed point ξ on the boundary to the current point Γ of the boundary under the sign of integral. $\partial/\partial n$ denotes the derivative in the direction of the outward normal to the boundary at that point Γ; $U(\Gamma)$ is the voltage at the current point of the boundary, and $U_{n}(\Gamma)$ is its normal derivative.

For a medium of homogeneous resistance, either the voltage U or its normal derivative U_{n} is specified at each point of the boundary. (This is true for external boundaries in case of a multi-phase medium.) An interpolation function is assumed between the nodes. In this work we applied a linear interpolation. Continuous linear elements with the nodes at the ends of the element are used. Thus, it is assumed that the voltage and its normal derivative have a linear evolution along the elements, except the points with sharp angles, where the derivative may have a jump. The curvilinear grain–void interface was approximated by segments of a straight line. Formally, this leads to sharp angles at the joints. However, since the original boundary is smooth and the 'sharpness' is very small, no jump of the derivative is assumed at these nodes. The discontinuity of the normal derivative is allowed only at the triple points A and B and at the right angles A_0, B_0, F and G.

The interpolation makes it possible to replace the integrals by sums, and the integral equation (40) becomes a linear set. Its solution yields the values of the voltage where its derivative was initially specified, and the values of the derivative where the voltage was set. On the internal boundaries between the phases of different conductivities we can establish both the voltage and its derivative. In particular, we establish the voltage U at each node of the curvilinear grain–void interface, and then approximate its second derivative with respect to the arclength U_{ss} by applying the central differences. Forward and backward differences are applied at triple points.

The resistance of the void was assumed infinite in the numerical simulations below. In this study, we followed the methodology described by Paris and Canas in [6] and used the codes supplied with this book.

Once the unknown grid values of the voltage derivative U_{n} are established along the vertical boundaries of the interconnect, its estimated total resistance becomes

$$R = \frac{U^{+} - U^{-}}{k_{g} \int_{h} U_{n}\, dy}, \tag{41}$$

where k_{g} is the specific electric conductivity of the grain material, $U^{+} - U^{-}$ is the external voltage applied to the interconnect and h is the path of the integration. Either the left or the right vertical boundary of the interconnect can be used. The result is the same up to the sign. Indeed, we apply the First Green Identity to the governing PDE (38)

$$\int \int_{\Omega} (\nabla k \cdot \nabla U + k \nabla^{2} U)\, d\Omega = \oint k U_{n}\, ds. \tag{42}$$

We get that the circulation of the electric current around the contour of the interconnect vanishes

$$\oint kU_{\mathrm{n}}\,\mathrm{d}s = 0. \tag{43}$$

In particular, Eq. (43) holds for the Laplace equation with $k = \text{const}$. A multi-phase medium with specific piecewise-constant conductivity can be considered as a special case of a medium with varying conductivity. Since along the horizontal sides of the interconnect U_{n} vanishes due to the boundary conditions, any vertical side can be used to establish resistance. The left side, where U^{+} is applied and $U_{\mathrm{n}}(y)$ is positive, gives a positive value of resistance. Since the field problem is linear, the resistance varies as the front evolves and it is independent of the applied voltage. We use Ohm's law to calculate the resistance.

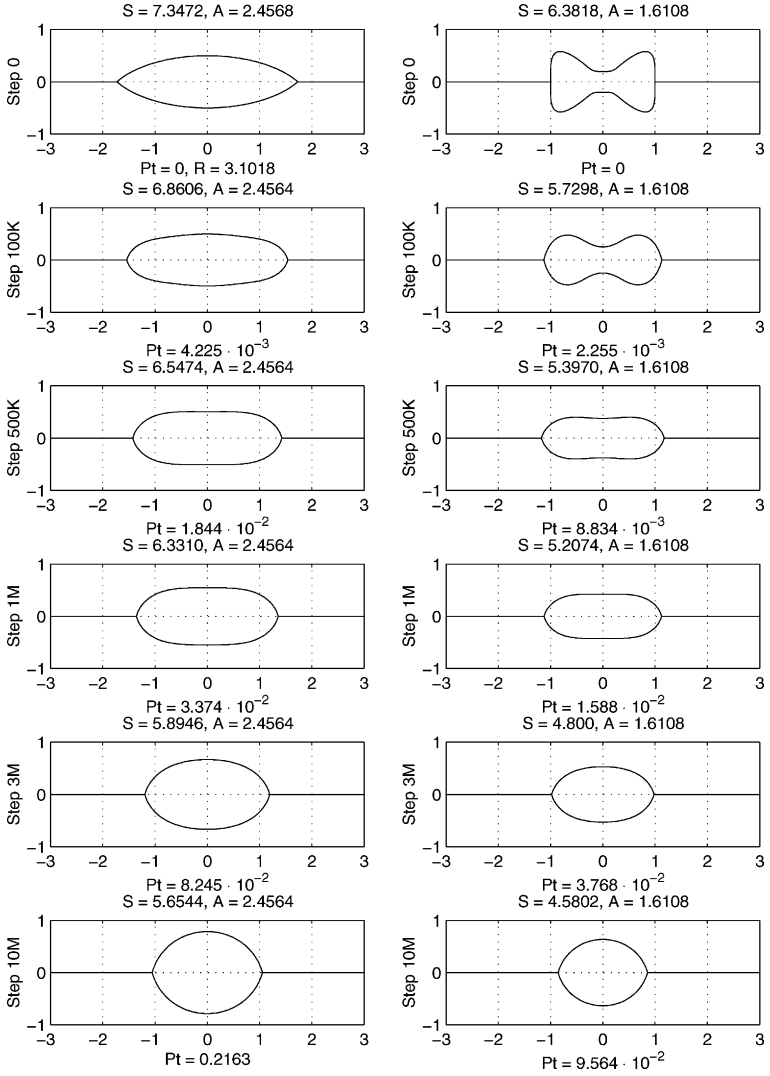

Fig. 4. Motion of elliptic arc and butterfly contour under diffusion forces.

6. Numerical simulation

In this section we present the results of three sets of simulations. The first set displays the interface motion under surface diffusion only. The second set combines the surface diffusion with electromigration forces for a void inside of a single grain. The third set presents electromigration of an intergranular void. Different initial configurations and ratios between the diffusion and electric field forces were studied.

For all cases, the grid has 100 intervals for the curvilinear boundary and 200 intervals for the total circumference of the interconnect. The size of the interconnect line for the set presented in Fig. 4 is 6×2 while it is 12×4 for the other sets. The voltage applied to the vertical sides is 12, so that the external field is of unit strength. Resistance of the void is assumed infinite.

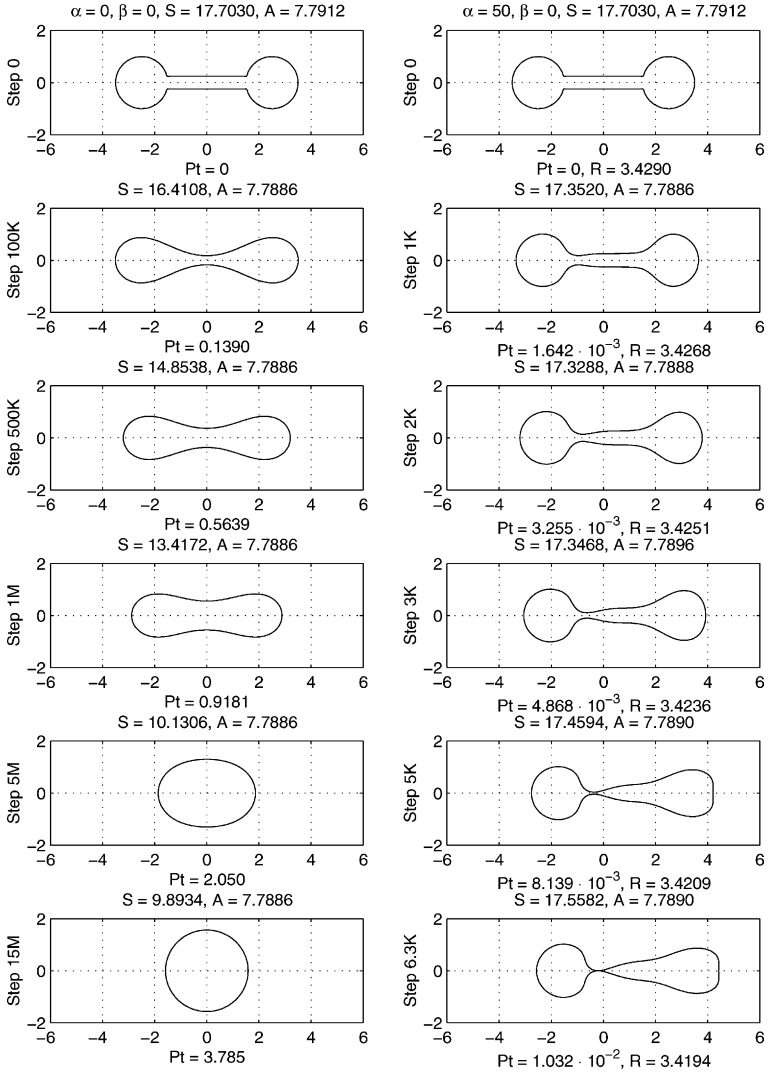

Fig. 5. Dumbbell void inside a single grain. Left column: $\alpha = \beta = 0$. Right column: $\alpha = 50$, $\beta = 0$.

6.1. Motion under diffusion forces only

Motion under the surface diffusion only is illustrated in Fig. 4 for two initial configurations: elliptic arc (left column) and butterfly contour (right column). The boundary conditions are $K_s = 0$ and $\Theta = 7\pi/12$. No external electric field was applied. In the beginning the triple angles were different from those required by the boundary condition. After 10 million steps we arrive to a figure that preserves the area and has the minimum perimeter for the given boundary conditions (angles at triple points). If $\Theta = \pi/2$, then the resulting figure is a circle.

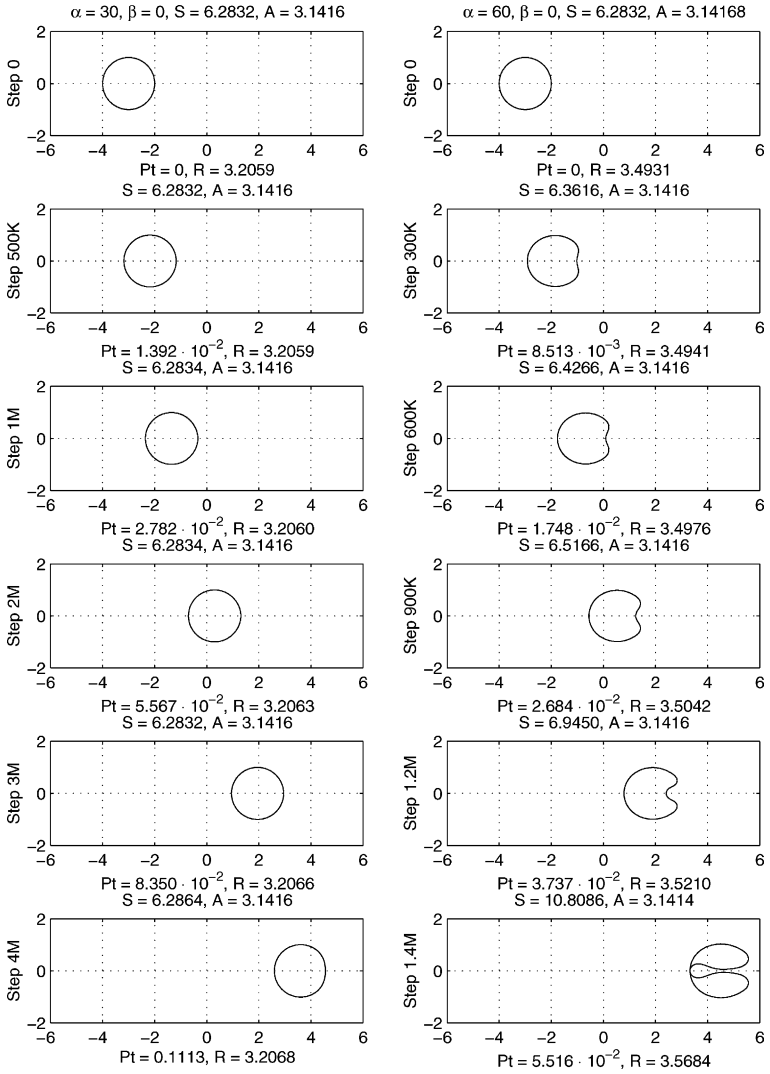

Fig. 6. Circular void inside a single grain. Left column: $\alpha = 30$, $\beta = 0$. Right column: $\alpha = 60$, $\beta = 0$.

6.2. Motion under diffusion and electric field

Motion of a symmetric void inside a single grain reduces to a particular case of the intergannular void problem. If the axis of symmetry coincides with the direction of the external field, then due to continuity, at the triple points $\Theta = \pi/2$ and the derivative of curvature vanishes: $K_s = 0$. Motion of the void with the initial Dumbbell configuration is presented in Fig. 5. In the left column, the void interface moves under the surface diffusion forces only. In the right column, the void motion under the surface diffusion and electric field is presented. The results are in good agreement with the results in [7] that were computed using the level set method.

We consider also the motion of a circular void studied by Xia et al. [8] with the finite element method. The radius of the void is unity, and for $\alpha = 30$ the void migrates in the direction of the electric field vector

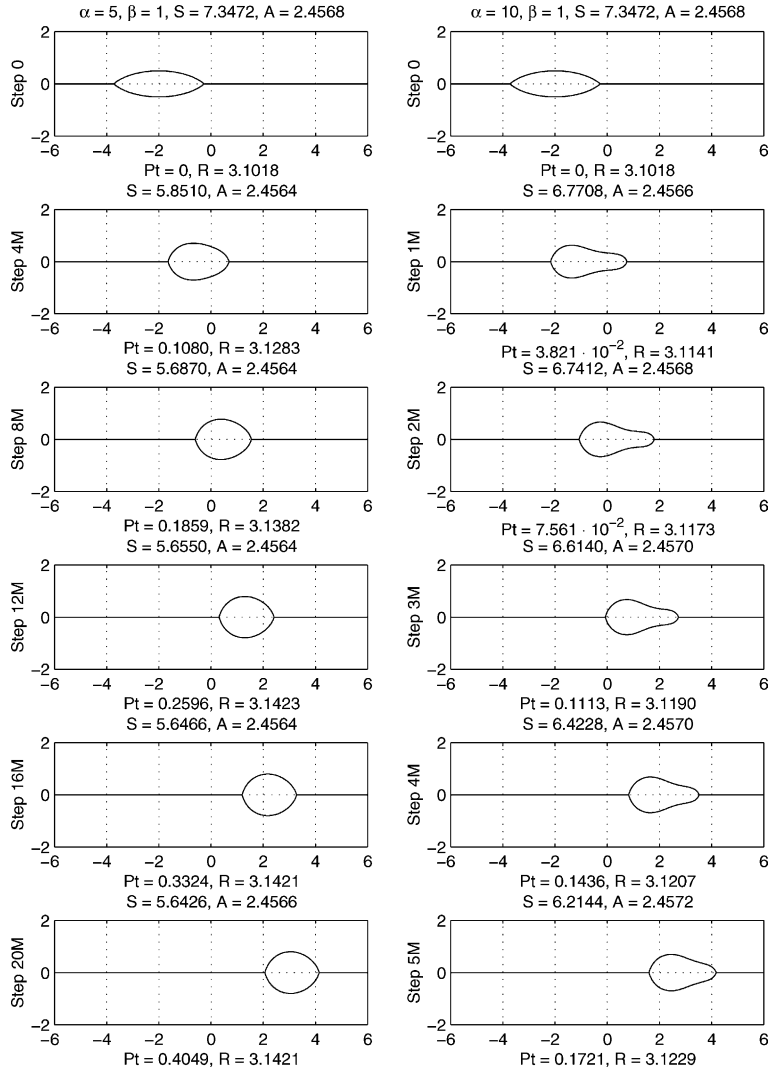

Fig. 7. Evolution of elliptic arc in weak and moderate fields. Left column: $\alpha = 5$, $\beta = 1$. Right column: $\alpha = 10$, $\beta = 1$.

and remains circular. For $\alpha = 60$ the void splits into two pieces, Fig. 6. The results are in good agreement with the finite element solution of [8].

6.3. Electromigration of intergranular void

Electromigration of intergranular void with the initial shape of an elliptic arc was studied for different ratios between the diffusion and electric field forces. In Fig. 7 a moderate field was modeled. The left column corresponds to $\alpha = 5$, $\beta = 1$, and the right column corresponds to $\alpha = 5$, $\beta = 1$. In Fig. 8 the motion is considered for the strong field with different influence of the boundary condition for the derivative of curvature: $\alpha = 20$, $\beta = 1$ in the left column and $\alpha = 20$, $\beta = 100$ in the right column. The factor β amplifies the influence of the electric field: increases the drift velocity of the void and leads to a faster split. The grid is the same as for the circular void.

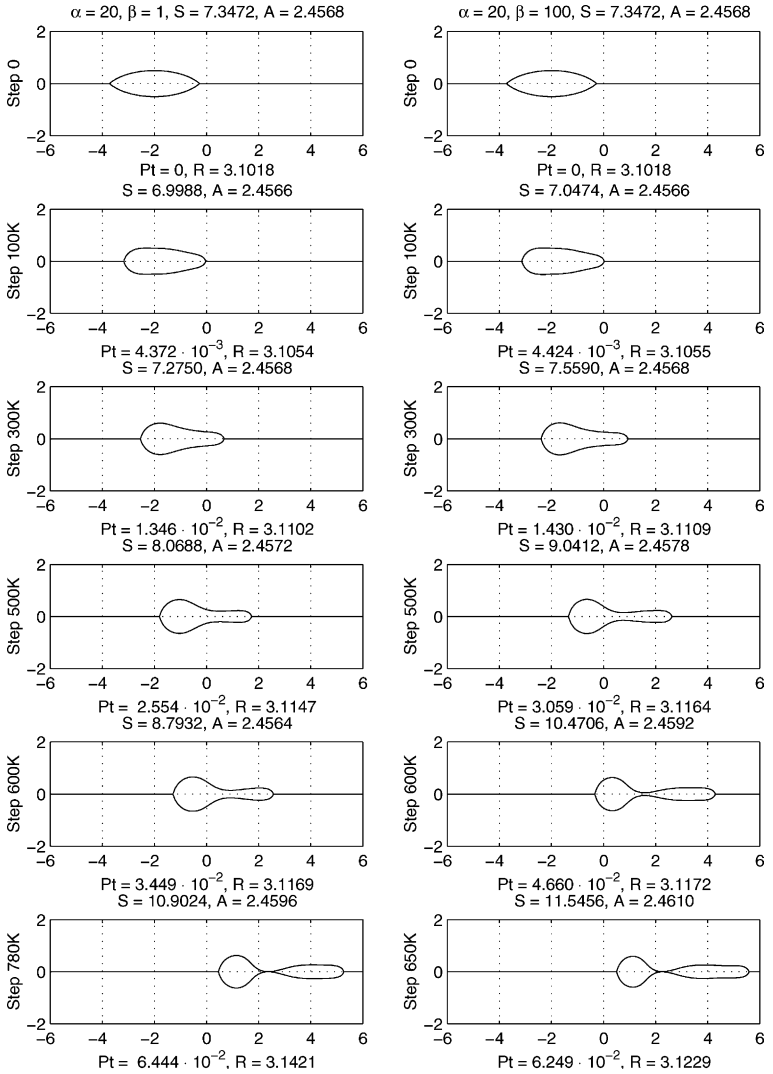

Fig. 8. Evolution of elliptic arc in strong field. Left column: $\alpha = 20$, $\beta = 1$. Right column: $\alpha = 20$, $\beta = 100$.

7. Summary

A computational methodology was developed and tested for the simulation of grain–void interface dynamics in metallic-film interconnects of microelectronic circuits. The motion of the interface under surface diffusion and electric field forces was studied. We did not take into consideration the elastic stress. The resistance of the substrate was assumed infinite.

A finite difference discretization in space and a second-order Runge–Kutta scheme in time were applied to solve a set of two coupled fourth-order governing PDEs. The low order of the Runge–Kutta scheme is justified, since the value of the time step is kept fairly small to satisfy stability requirements. The initial location of the front has to be specified for the governing time-dependent PDEs. The boundary conditions include slopes of the interface line and derivatives of its curvature with respect to the arclength.

It cannot be denied that the two-dimensional level set method is a more general approach and gives solutions for more sophisticated electromigration topology than the one-dimensional formulation applied in this study. However, for the specific problem considered here, the Cartesian formulation becomes an effective and attractive alternative. In particular, we get the solution immediately at the generating points of the interface line and need not to apply a two-dimensional interpolation in space to update the location of the interface. Thus, the interpolation error is avoided.

The boundary element method was applied to solve the Laplace equation for the voltage distribution. This method is especially convenient for the curvilinear boundary since we need the potential values only on the contour line. The variation of the total resistance of the interconnect with time was examined. This value can be further used as an interconnect failure criterion.

The electrostatic problem is the 'bottleneck' of the numerical simulation, and consumes most of the computational time, because the resolving matrix of the boundary element formulation is dense. In this study we applied the Gauss elimination procedure to solve the boundary element set. However, the direct solver cannot use the availability of the initial guess from the previous time step. Iterative methods use effectively such an input, and thus they can be recommended.

Since the time step of the explicit scheme for the fourth-order PDEs is fairly small, the field may be updated periodically once per several time steps without significant loss of accuracy.

Numerical simulations were run for various initial configurations and various ratios between diffusion and field forces.

References

[1] O. Kraft, E. Arzt, Numerical simulation of electromigration-induced shape changes of voids in bamboo lines, Applied Physics Letters 66 (16) (1995) 2063–2065.
[2] L. Klinger, L. Levin, Morphological stability of a heterophase interface under electromigration conditions, Journal of Applied Physics 79 (9) (1996) 6834–6839.
[3] L.M. Klinger, X. Chu, W.W. Mullins, C.L. Bauer, Grain-boundary slit propagation in an electric field, Journal of Applied Physics 80 (12) (1996) 6670–6676.
[4] H.K. Zhao, T.F. Chan, B. Merriman, S. Osher, A variational level set approach to multiphase motion, Journal of Computational Physics 127 (1996) 179–195.
[5] J.A. Sethian, Level Set Methods, Evolving Interfaces in Geometry, Fluid Mechanics, Computer Vision and Materials Science, Cambridge University Press, Cambridge, 1996.
[6] F. Paris, J. Canas, Boundary Element Method. Fundamentals and Applications, Oxford Science Publications, 1997.
[7] A. Averbuch, M. Israeli, I. Ravve, I. Yavneh, Computation for electromigration in interconnects of microelectronic devices, Journal of Computational Physics 167 (2001) 316–371.
[8] L. Xia, A.F. Bower, Z. Suo, C.F. Shih, A finite element analysis of the motion and evolution of voids due to strain and electromigration induced surface diffusion, Journal of the Mechanics and Physics of Solids 45 (9) (1997) 1473–1493.
[9] Y.W. Zhang, A.F. Bower, L. Xia, C.F. Shih, Three dimensional finite element analysis of the evolution of voids and thin films by strain and electromigration induced surface diffusion, Journal of the Mechanics and Physics of Solids 47 (1999) 1473–1493.

[10] Y.W. Zhang, A.F. Bower, Three dimensional simulations of island formation in a coherent strained epitaxial film, Thin Solid Films 357 (1999) 8–12.
[11] O. Kraft, M. Hommel, E. Arzt, X-ray diffraction as a tool to study the mechanical behavior of thin films, Materials Science and Engineering A 288 (2000) 209–216.
[12] M.R. Gungor, D. Maroudas, Theoretical analysis of electromigration-induced failure of metallic thin films due to transgranular void propagation, Journal of Applied Physics 85 (4) (1999) 2233–2246.
[13] M.R. Gungor, D. Maroudas, Modeling of electromechanically induced failure of passivated metallic thin films used in device interconnections, International Journal of Fracture 109 (2001) 47–68.
[14] M. Schimschak, J. Krug, Electromigration-driven shape evolution of two-dimensional voids, Journal of Applied Physics 87 (2) (2000) 695–703.
[15] M. Mahadevan, R.M. Bradley, J.M. Debierre, Simulations of an electromigration-induced edge instability in single-crystal metal lines, Europhysics Letters 45 (1999) 680–685.
[16] J.B. Collins, Diffuse interface model of diffusion-limited crystal growth, Physical Review B 31 (1985) 6119–6122.
[17] D.N. Bhate, A. Kumar, A.F. Bower, Diffuse interface model for electromigration and stress voiding, Journal of Applied Physics 87 (4) (2000) 1712–1721.
[18] J.W. Cahn, J.E. Hilliard, Free energy of a nonuniform system. I. Interfacial free energy, The Journal of Chemical Physics 28-2 (1958) 258–267.
[19] D.R. Fridline, A.F. Bower, Influence of anisotropic surface diffusivity on elctromigration induced void migration and evolution, Journal of Applied Physics 85 (6) (1999) 3168–3174.
[20] O. Kraft, E. Arzt, Electromigration mechanisms in conductor lines: void shape changes and slit-like failure, Acta Materialia 45 (4) (1997) 1599–1611.
[21] R. Spolenak, O. Kraft, E. Arzt, Effects of alloying elements on electromigration, Microelectronics Reliability 38 (1998) 1015–1020.
[22] O. Kraft, E. Arzt, Current density and line width effects in electromigration: a new damage-based life time model, Acta Materialia 46 (11) (1998) 3733–3743.
[23] D. Maroudas, M.R. Gungor, Continuum and atomistic modeling of electro mechanically-induced failure of ductile metallic thin films, Computational Materials Science 23 (2002) 242–249.
[24] D. Fridline, A. Bower, Numerical simulations on stress induced void evolution and growth in interconnects, Journal of Applied Physics 91 (4) (2002) 2380–2390.
[25] M.R. Gungor, D. Maroudas, L.J. Gray, Effects of mechanical stress on electromigration-driven transgranular void dynamics in passivated metallic thin films, Applied Physics Letters 73 (26) (1998) 3848–3850.
[26] M.R. Gungor, D. Maroudas, Electromigration-induced failure of metallic thin films due to transgranular void propagation, Applied Physics Letters 72 (26) (1998) 3452–3454.
[27] M. Schimschak, J. Krug, Electromigration-induced breakup of two-dimensional voids, Physical Review Letters 80 (8) (1998) 1674–1677.
[28] M. Schimschak, J. Krug, Surface electromigration as a moving boundary value problem, Physical Review Letters 78 (2) (1997) 278–281.
[29] M. Mahadevan, R. Mark Bradley, Simulations and theory of electromigration-induced slit formation in unpassivated single-crystal metal lines, Physical Review B 59 (16) (1999) 11037–11046.
[30] D.N. Bhate, A.F. Bower, A. Kumar, A phase field model for failure in interconnect lines due to coupled diffusion mechanisms, Journal of the Mechanics and Physics for Solids 50 (2002) 2057–2083.
[31] M.R. Gungor, D. Maroudas, Current-induced non-linear dynamics of voids in metallic thin films: morphological transition and surface wave propagation, Surface Science 461 (2000) L550–L556.
[32] M.R. Gungor, D. Maroudas, Nonhydrostatic stress effects on failure of passivated metallic thin films due to void surface electromigration, Surface Science 432 (1999) L604–L610.
[33] M.R. Gungor, D. Maroudas, Non-linear analysis of the morphological evolution of void surfaces in metallic thin films under surface electromigration conditions, Surface Science 415 (1998) L1055–L1060.
[34] L.J. Gray, D. Maroudas, M.N. Enmark, E.F. Azevedo, Approximate Green's functions in boundary integral analysis, Engineering Analysis with Boundary Elements 23 (1999) 267–274.
[35] Z. Suo, Evolving material structures of small feature sizes, International Journal of Solids and Structures 37 (2000) 367–378.
[36] Z. Suo, Stable state of interconnect under temperature change and electric current, Acta Materialia 46 (11) (1998) 3725–3732.
[37] H.H. Yu, Z. Suo, An axisymmetric model of pore-grain boundary separation, Journal of the Mechanics and Physics of Solids 47 (1999) 1131–1155.
[38] B. Sun, Z. Suo, C.F. Cocks, A global analysis of structural evolution in a row of grains, Journal of the Mechanics and Physics of Solids 44 (4) (1996) 559–581.
[39] B. Sun, Z. Suo, W. Yang, A finite element method for simulating interface motion – I. Migration of phase and grain boundaries, Acta Materialia 45 (5) (1997) 1907–1915.

[40] B. Sun, Z. Suo, A finite element method for simulating interface motion – II. Large shape change due to surface diffusion, Acta Materialia 45 (12) (1997) 4953–4962.
[41] D. Adalsteinsson, J.A. Sethian, A level set approach to a unified model for etching, deposition and lithography I: algorithms and two-dimensional simulations, Journal of Computational Physics 120 (1995) 128–144.
[42] D. Adalsteinsson, J.A. Sethian, A level set approach to a unified model for etching, deposition and lithography II: three-dimensional simulations, Journal of Computational Physics 122 (1995) 348–366.
[43] J.A. Sethian, D. Adalsteinsson, An overview of level set methods for etching, deposition, and lithography development, IEEE Transactions on Semiconductor Manufacturing 10 (1) (1997) 167–184.
[44] H. Zhao, T. Chan, B. Merriman, S. Osher, A variational level set approach to multiphase motion, Journal of Computational Physics 127 (1996) 179–195.